Key Engineering Materials
ISSN: 1662-9795, Vol. 984, pp 55-62
doi:10.4028/p-T0xLa9

Submitted: 2023-09-08
Accepted: 2024-04-12
Online: 2024-08-22

Device Modeling of 4H-SiC PIN Photodiodes with Shallow Implanted Al Emitters for VUV Sensor Applications

Michael Schraml[1,a*], Mathias Rommel[1,b], Niklas Papathanasiou[2,c] and Tobias Erlbacher[3,4,d]

[1]Fraunhofer Institute for Integrated Systems and Device Technology IISB, Schottkystrasse 10, 91058 Erlangen, Germany

[2]sglux GmbH, Richard-Willstätter-Str. 8, 12489 Berlin, Germany

[3]Friedrich-Alexander-Universität Erlangen-Nürnberg, Chair of Electron Devices, Cauerstrasse 6, 91058 Erlangen, Germany

[4]Nexperia Germany GmbH, Stresemannallee 101, 22529 Hamburg, Germany

[a]michael.schraml@iisb.fraunhofer.de, [b]mathias.rommel@iisb.fraunhofer.de, [c]papathanasiou@sglux.de, [d]tobias.erlbacher@nexperia.com

Keywords: photodiode, vacuum UV, shallow ion-implantation, photoresponsivity, numerical simulation

Abstract. A numerical model is presented for the simulation of ultraviolet ion-implanted 4H-SiC photodiodes with shallow p^- emitter doping profiles. An existing model for SiC pin photodiodes, taken from literature, is modified with a dedicated SiO_2-SiC interface layer to account for degradation of carrier mobility and lifetime at the interface. Furthermore, aluminum compensation in 4H-SiC is included and its impact on the spectral response and carrier recombination is analyzed. The simulated spectral response in the wavelength range from 200 to 400 nm is compared to experimental data. While the existing model, taken from literature, fails to predict the performance of VUV photodiodes with a shallow p^- emitter, the newly designed model successfully achieves high accuracy, even with a basic modeling approach featuring an abrupt material parameter transition.

Introduction

Vacuum ultraviolet light (VUV) is the wavelength range from 10 to 200 nm [1] and photon detection in this range is important for high resolution semiconductor lithography [1], space science [1], solar observations [2] as well as radiation monitoring. For example, Xenon excimer radiation has a peak emission at a wavelength of 172 nm [3]. In general, silicon carbide (SiC) offers optimal conditions for ultraviolet (UV) photodiodes due to its wide band gap of 3.26 eV [4] in the case of the 4H polytype. This results in a cut-off wavelength of 380 nm, allowing visible blind photodiodes without the need for optical filters. Due to the low intrinsic carrier concentration, SiC pn diodes have an extremely low reverse dark current [4] and the associated noise is orders of magnitude lower than that of silicon photodetectors [4]. The high thermal conductivity (up to 4.9 W cm^{-1} K^{-1} [4]) and chemical stability [4] also makes SiC-based photodiodes suitable for harsh environments.

To date, only SiC Schottky photodiodes are capable of detecting VUV with a reasonable sensitivity [5, 6]. However, Schottky-based diodes exhibit a higher dark current at elevated temperatures [7], and the use of a front metal can reduce the overall sensitivity due to the absorption of the UV light in the top metal contact. In our previous work [8], we had investigated 4H-SiC pin photodiodes with different shallow aluminum (Al) ion-implanted p^- emitter profiles for their ability to detect VUV radiation. We were able to significantly increase the sensitivity at a wavelength of 200 nm by using an appropriate emitter doping profile, but the overall sensitivity in the spectrum from 200 to 400 nm remained weak. Understanding the device behavior is crucial for further optimization of VUV sensitive SiC photodiodes and, therefore, a new semiconductor device model for Sentaurus TCAD is presented and compared to electro-optical measurement results.

Device Manufacturing and Measurements

The structure of the vertical 4H-SiC VUV pin photodiode is shown in Fig. 1. The diodes were fabricated according to the process presented in our previous work using a 6 µm thick epitaxial layer with a nitrogen doping concentration of $9.2 \cdot 10^{14}$ cm^{-3} as an intrinsic layer. The p emitter regions were formed with the as-implanted aluminum emitter doping profiles in Fig. 2, obtained by secondary ion mass spectroscopy and Monte-Carlo simulation in Sentaurus Process [9]. The shallow doping profiles Em1 and Em2 are used for potential VUV-sensitive photodiodes as p^- emitters, while the profile Em3 is used as a p^+ contact doping profile to ensure proper ohmic contact formation under the contact pad and outer contact ring. The reference UV photodiode without VUV sensitivity uses only the Em3 doping profile for both, the entire active area and for the ohmic contact regions. In the following, the diodes are referred to by their respective doping profile names for simplicity. In this work, diodes with a 30 nm antireflective coating (ARC) formed by dry thermal oxidation and annealed in NO are investigated. The active area is 2.0 mm².

The spectral response (SR) measurements in the 200 to 390 nm wavelength range were performed using a 150 W xenon light source, a double monochromator, and a calibrated SiC photodiode as a reference diode. Details of the measurement setup can be found here [8].

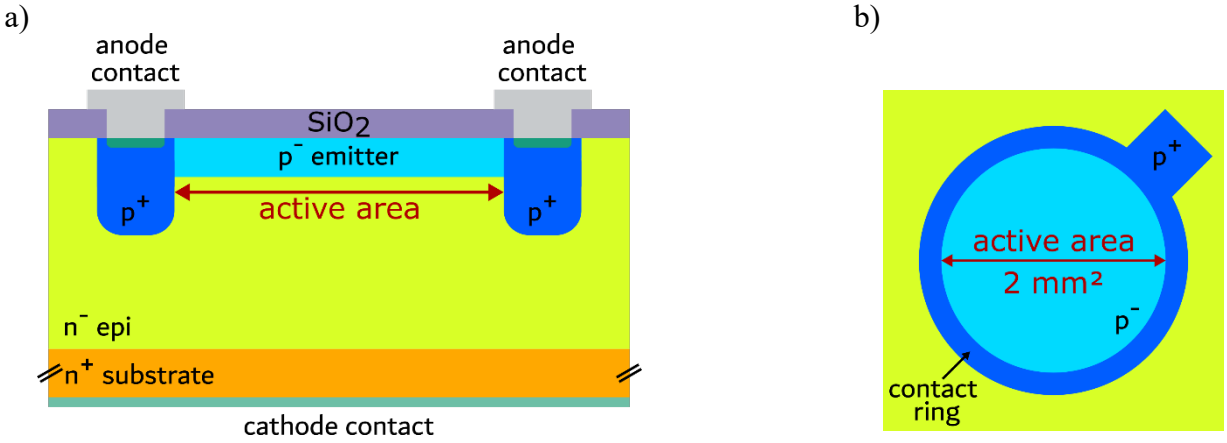

Fig. 1 Diode structure in a) cross section view and b) implantation pattern in top view of the investigated VUV photodiodes

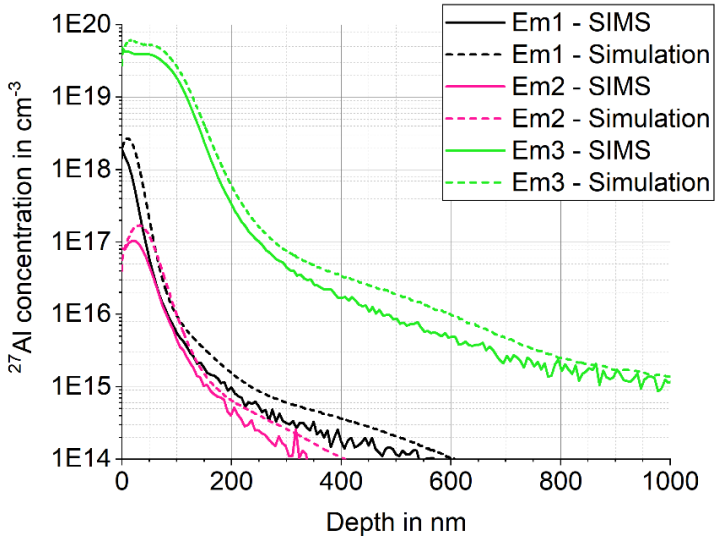

Fig. 2 Aluminum profiles used for p emitter formation determined by SIMS and Monte-Carlo simulation

Numerical Simulation Model

First, the photo-responsivity of the 4H-SiC photodiodes was simulated using Synopsys Sentaurus Device [10] (version U-2022.12) and the model presented by Burenkov et al. [11]. The device structure was built with Sentaurus Structure Editor [12] according to the manufactured diode. Due to the symmetry, a 2D simulation of one half of the diode is sufficient. The device parameters are listed in Table 1. The simulated doping profiles in Fig. 2 were used as p^- and p^+ doping profiles.

For the electrical and optical simulation, Fermi statistics, band gap narrowing with the Jain-Roulston model, incomplete ionization of Al and N impurities and the charge carrier transport model as implemented in Sentaurus Device were used. The parameters for the doping dependent charge carrier recombination of Burenkov et. al [11] were used. This model assumes an effective carrier lifetime that is equal for electrons and holes. For the doping dependent mobility, maximum mobilities of 380 and 70 $cm^2\ (Vs)^{-1}$ for the electrons and holes, respectively, were applied. The complex refractive index used for the optical simulation was calculated from the ordinary component of the dielectric function of 4H-SiC taken from Lindquist et al. [13]. The optics were calculated using the transfer matrix method solver. As an excitation, a monochromatic, unpolarized light with an intensity of 1.0 $\mu W\ cm^{-2}$ was used to determine the responsivity in the wavelength range from 200 to 400 nm.

In addition to investigating the predictions of the Burenkov model with respect to measurements, a modification of the Burenkov model is presented in this work. The modification introduces a dedicated layer at the SiO_2-SiC interface with constant, low values for carrier mobilities and lifetimes, see Table 2. Thus, the degradation of the carrier lifetime due to the surface recombination at interface states as well as the low carrier mobility at the SiO_2-SiC interface [4] are explicitly considered. The doping-dependent parameter values of the mobility and lifetime coming from the Burenkov model are overwritten in this interface layer, but outside, the standard Burenkov model is applied. This leads to abrupt transitions in the carrier mobilities and lifetimes, but nevertheless, the model allows a better understanding of the device behavior. Furthermore, the aluminum compensation effects [14] are implemented by globally reducing the active aluminum doping concentration throughout the whole device by a constant compensation ratio given in Table 2.

Table 1 Device parameters used for the simulation

Parameter	value
Total width of the diode	817 um
Width of the electrical contact	20 um
Thickness of the n^- epi layer	6.1 um
Doping concentration of the n^- epi layer	$9.23 \cdot 10^{14}\ cm^{-3}$
Thickness of the n^+ substrate	50 um
Doping concentration of the n^+ substrate	$1.0 \cdot 10^{18}\ cm^{-3}$
Thickness of SiO_2 ARC layer	30 nm

Table 2 Parameter set for the model of this work with a dedicated SiO_2-SiC interface layer

Parameter	value
Global Al compensation ratio	85%
Layer thickness	200 nm
Effective carrier lifetime	$1 \cdot 10^{-14}$ s
Electron mobility	$1.0\ cm^2\ (Vs)^{-1}$
Hole mobility	$0.23\ cm^2\ (Vs)^{-1}$

Results and Discussion

Fig. 3 shows the spectral response as obtained by the Burenkov model, the modified model with the interface layer and Al compensation (hereinafter referred to as *this work*) and experimental measurements. The Burenkov model predicts the behavior of the reference UV photodiode (Em3) well. It fails, however, in predicting the responsivity of the VUV diodes with the shallow emitter profiles Em1 and Em2. The model drastically overpredicts the responsivity for the profile Em2 across the whole spectrum and for wavelengths below 310 nm in case of the profile Em1. This can be explained by an overestimated surface passivation in the Burenkov model. Thus, carrier lifetime and mobility degeneration at the SiO_2-SiC interface are not sufficiently considered. In the case of the UV reference diode, the doping-dependent models for the carrier mobilities and lifetimes already lead to

lower mobilities and lifetimes at the interface due to the high doping concentrations of the profile Em3, as can be seen in Fig. 4 and 5. Therefore, the Burenkov model is accurate for the UV reference diode compared to the experimental data.

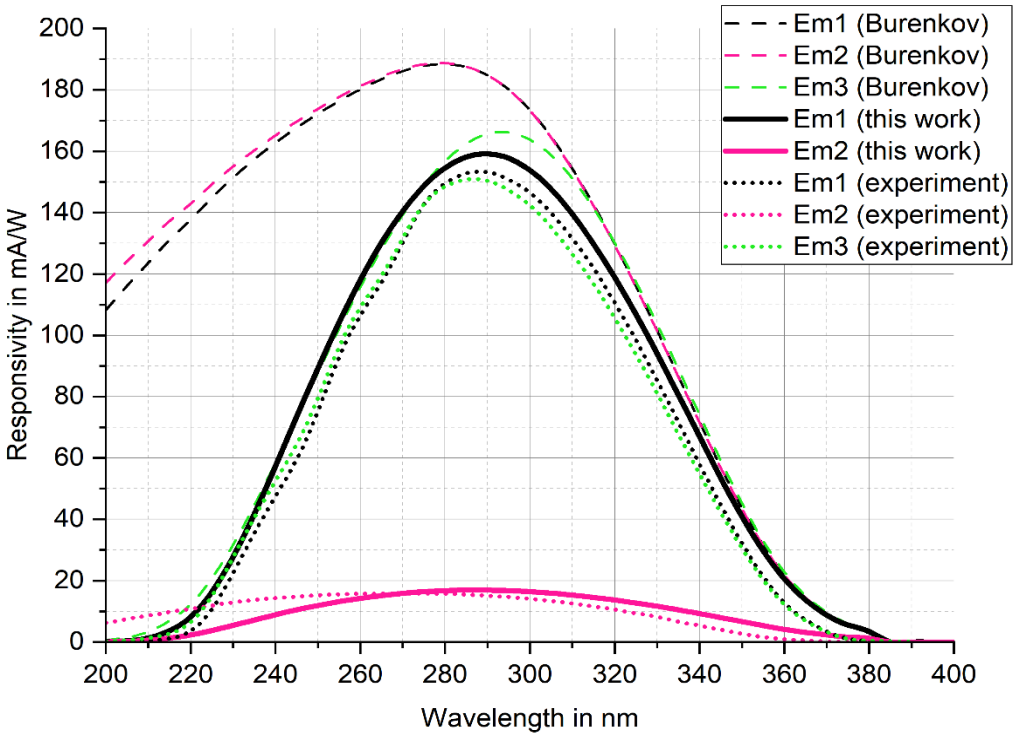

Fig. 3. Spectral response of the Burenkov model, the modified model of this work, and the experimental data of the (V)UV photodiodes

In order to account for the carrier lifetime and mobility degradation at the SiO_2-SiC interface for the VUV diodes with shallow doping profiles, the SiO_2-SiC interface layer was implemented as presented in the previous section. The trust-region reflective least-squares algorithm [15] as implemented in Sentaurus Workbench Optimization Framework [16] and manual adjustments were used to find an optimal set of parameters for the interface layer to match the experimental SR data. The interface layer parameters are shown in Table 2 and are used for the shallow doping profiles Em1 and Em2. Besides the low parameter values for the carrier lifetimes and mobilities, a high, globally applied Al compensation of 85% is used. According to literature, the compensation can be assumed to be as high as 84% for low doped Al regions [14], hence the compensation used in this work is still plausible. The new model of this work can accurately predict the behavior of the two shallow profiles Em1 and Em2 (cf. Fig. 3), only the response for wavelengths below 260 nm is too small for the profile Em2 compared to the experimental data. The depth dependent effective carrier lifetimes are shown in Fig. 4. The Burenkov model calculates a lifetime of less than $1 \cdot 10^{-13}$ s at the interface to the SiO_2 layer for Em3 while the values for Em1 and Em2 are between $1 \cdot 10^{-11}$ s and $1 \cdot 10^{-9}$ s. A similar behavior can be seen for the carrier mobility, which is shown as an example for electrons in Fig. 5. The hole mobility would show the same doping dependence only with a maximum mobility of 70 $cm^2 (Vs)^{-1}$. Applying the new model with the interface layer and the Al compensation, a box profile with an abrupt transition for the lifetimes and mobilities is present, that is the same for both shallow profiles Em1 and Em2. The slight deviations between the Burenkov model and the model of this work at 200 nm and below for the electron mobility are due to the high global compensation ratio applied in the model of this work. Thus, the underlying doping dependence already reaches the maximum mobility values at 200 nm for both shallow doping profiles Em1 and Em2.

The influence of the interface layer on the spectral response is analyzed by looking at the Shockley-Read-Hall (SRH) recombination rate and the carrier generation rate due to photon absorption. The values are displayed in Fig. 6 and 7 for a wavelength of 200 nm and 285 nm, respectively. First, the recombination and generation rate at 200 nm will be discussed.

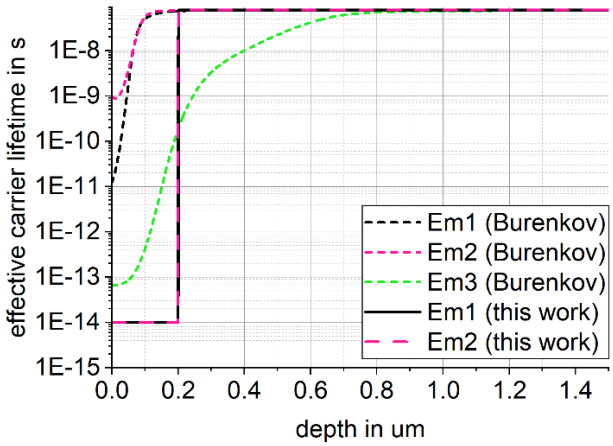

Fig. 4 Effective carrier lifetimes in SiC for electron and holes determined from the Burenkov model and this work. The values of Em1 (this work) and Em2 (this work) are identically in the interface layer, therefore the lines lie on top of each other

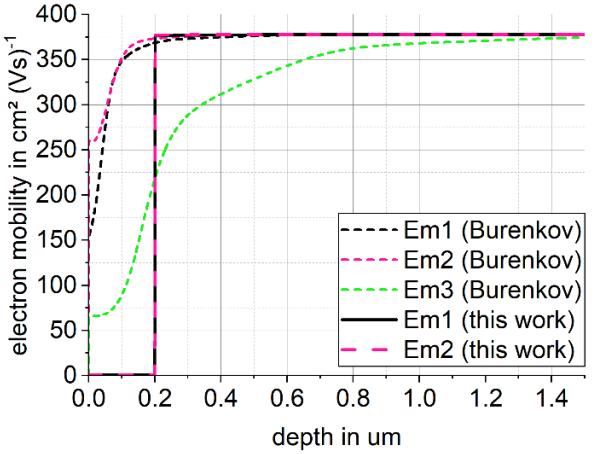

Fig. 5 Electron mobilities in SiC determined from the Burenkov model and this work. The values of Em1 (this work) and Em2 (this work) are identically in the interface layer, therefore the lines lie on top of each other

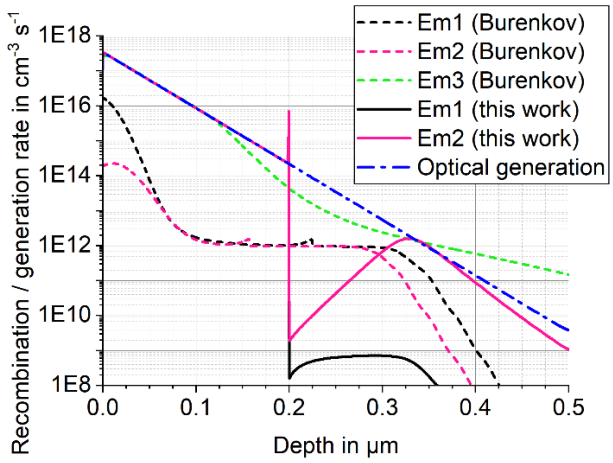

Fig. 6 SRH recombination rate and optical generation at a wavelength of 200 nm

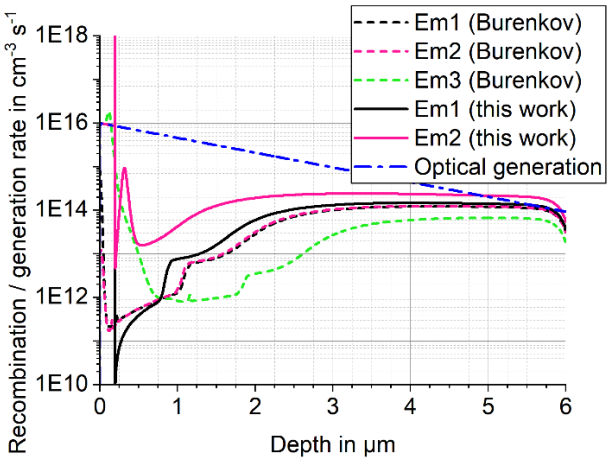

Fig. 7 SRH recombination rate and optical generation at a wavelength of 285 nm

The Burenkov model shows for the profile Em3 a recombination rate that is as high as the optical generation followed by a short region with a higher generation, which is again followed by a higher recombination than generation. Thus, almost all generated carriers recombine and the sensitivity for this wavelength is low (see Fig. 3). The Burenkov model shows for the shallow profiles Em1 and Em2 throughout the whole displayed depth a higher generation than recombination leading to the high sensitivity for that wavelength since more carriers are generated than recombine. With the introduction of the interface layer, in the first 200 nm for both shallow emitter profiles, Em1 and Em2, the recombination is as high as the generation. Below the interface layer, the recombination is smaller than the generation, but the optical generation is already 3 orders of magnitude smaller. Therefore, the remaining carrier generation below the interface layer can be neglected. Thus, these profiles also show a low response at 200 nm.

At a wavelength of 285 nm, the Burenkov model has a recombination rate for the first 150 nm that is equal to or even greater than the optical generation rate for the profile Em3. Below that, the recombination rate is less than the generation rate for the entire intrinsic layer, which explains the high responsivity at this wavelength. For the profiles Em1 and Em2 with the Burenkov model, the recombination is always smaller than the generation throughout the intrinsic layer, which is responsible for the even higher sensitivity compared to the profile Em3. In the model of this work, the recombination is as high as the generation in the interface layer. Below this layer, the new model

also leads to higher recombination rates compared to the Burenkov model. This is particularly evident for the profile Em2. This can be attributed to the high compensation of the aluminum dopants, with a value of 85%. The high compensation ratio leads to a lower electric field within the space charge region due to the low doping concentration. Therefore, the generated electron-hole pairs remain in the device for a longer time and the chance of recombination increases. As a result, higher SRH rates are present and the responsivity over the entire wavelength range becomes low. This effect can be seen by looking at the SRH rates of different compensation ratios, which will be discussed in the subsequent paragraph.

The influence of the global compensation ratio on the spectral response and the SRH recombination at 285 nm are presented in Fig. 8 and 9. The analysis retains all other interface layer parameters at the best fit values listed in Table 2. The SR of the profile Em1, shows no significant dependence on the Aluminum compensation ratio up to 85%. The profile Em2 remains like the SR of the profile Em1 up to a compensation ratio of 65%. However, when the compensation ratio reaches 85%, the SR weakens and becomes closer to the experimental data (see Fig. 8b). The SRH recombination rate at 285 nm, as shown in Fig. 9, does not vary significantly for profile Em1 across the compensation ratios examined. The SRH recombination rate of the profile Em2 remains similar to Em1 for compensation ratios up to 65%, thus, explaining the comparable spectral response. At a compensation ratio of 85%, the profile Em2 shows higher recombination rates not only in the vicinity of the interface layer but throughout the entire intrinsic n^- layer, therefore leading to the weak response.

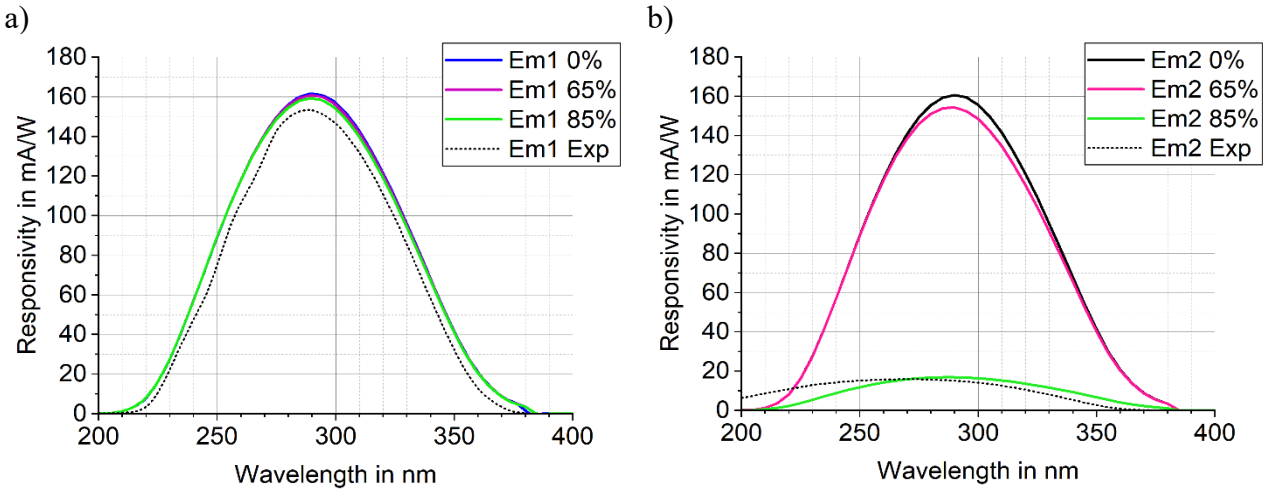

Fig. 8 Influence of the Aluminum compensation on the spectral response for the profile Em1 (a) and Em2 (b)

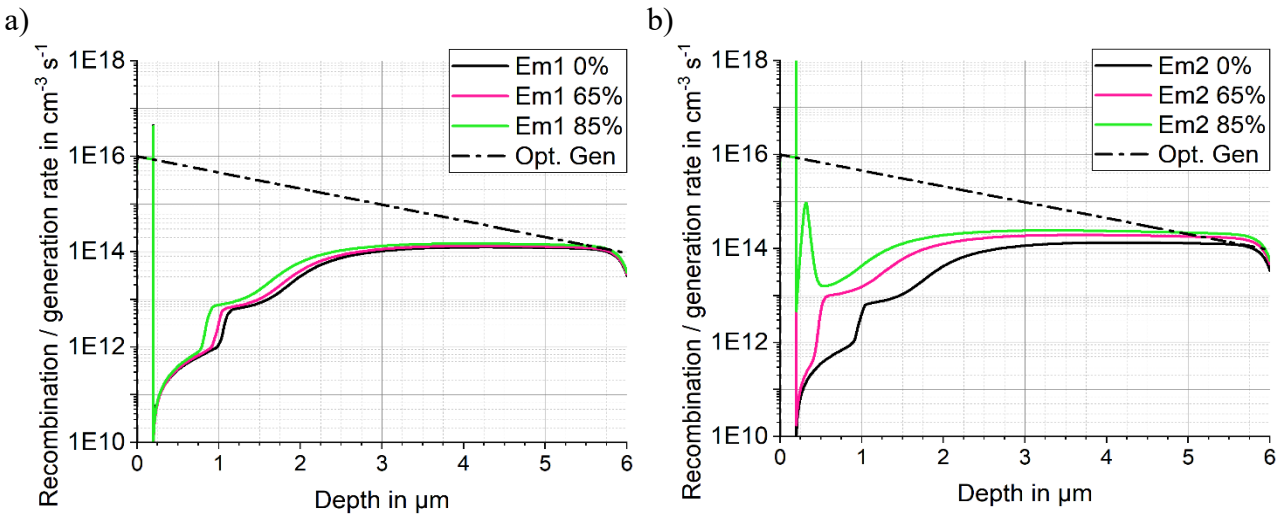

Fig. 9 Influence of the Aluminum compensation on the SRH recombination rate at a wavelength of 285 nm for the profile Em1 (a) and Em2 (b)

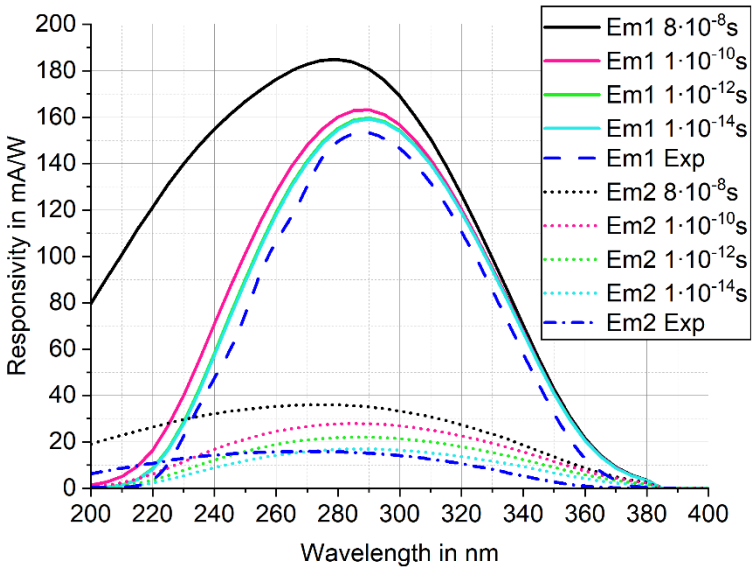

Fig. 10 Influence of the carrier lifetime in the interface layer on the spectral response

Similarly, the influence of the carrier lifetime in the interface layer on the spectral response was analyzed while keeping all other parameters as presented in Table 2. The SR results are shown in Fig. 10. A carrier lifetime of $8 \cdot 10^{-8}$ s results in an overestimation of the spectral response for both shallow profiles Em1 and Em2. Profile Em1 shows hardly any significant variation for lifetimes between $1 \cdot 10^{-10}$ s and $1 \cdot 10^{-14}$ s. Thus, if the carrier lifetime is small enough, its influence on the SR decreases. The profile Em2 shows a higher sensitivity to the carrier lifetime in the interface layer, with smaller lifetimes leading to even lower sensitivities over the entire wavelength range. Only a lifetime of $8 \cdot 10^{-8}$ s shows a sensitivity at 200 nm, while the shorter carrier lifetimes studied lead to no sensitivity at this wavelength. However, the best overall fit to the experimental data is given by the shortest lifetime investigated, $1 \cdot 10^{-14}$ s.

Conclusion

The simulation model from Burenkov et al. [11] is not able to predict the behavior of 4H-SiC pin photodiodes with shallow implanted p^- emitter doping profiles. By introducing a layer at the SiO_2-SiC interface with constant low carrier mobilities and lifetimes in combination with an appropriate aluminum compensation ratio, a high agreement with the experimental data was achieved. The presented model is still preliminary and unphysical due to the constant parameter values in the interface layer and the abrupt transitions of the carrier mobilities and lifetimes. Nevertheless, the most important parameters, namely both the aluminum compensation and the effective carrier lifetime in the interface layer, have been discussed in detail. To describe the different behavior of the diodes with the shallow doping profile, it is essential to consider a high compensation ratio of 85% for an accurate simulation as well as rather low carrier lifetimes of $1 \cdot 10^{-14}$ s at the SiO_2-SiC interface.

Further investigations need to focus on the physical refinement of the model without abrupt parameter value transitions. Moreover, it is important to investigate, whether the degradation of the carrier mobility and lifetime at the interface is solely an effect of the interface itself or whether there is a dependence on the doping concentration and thus ion-implantation dose. Therefore, further shallow doping profiles and different SiO_2 deposition techniques need to be studied.

Acknowledgement

This Project is supported by the Federal Ministry for Economic Affairs and Climate Action (BMWK) on the basis of a decision by the German Bundestag.

References

[1] L. Jia, W. Zheng, F. Huang, Vacuum-ultraviolet photodetectors, PhotoniX 1 (2020).

[2] K. Wilhelm, E. Marsch, B.N. Dwivedi, U. Feldman, Observations of the Sun at Vacuum-Ultraviolet Wavelengths from Space. Part II: Results and Interpretations, Space Sci Rev 133 (2007) 103–179.

[3] B. Eliasson, U. Kogelschatz, UV excimer radiation from dielectric-barrier discharges, Appl. Phys. B 46 (1988) 299–303.

[4] T. Kimoto, J.A. Cooper, Fundamentals of silicon carbide technology: Growth, characterization, devices and applications, Wiley, Singapore, 2014.

[5] A. Gottwald, U. Kroth, E. Kalinina, V. Zabrodskii, Optical properties of a Cr/4H-SiC photodetector in the spectral range from ultraviolet to extreme ultraviolet, Applied optics 57 (2018) 8431–8436.

[6] J. Hu, X. Xin, J.H. Zhao, F. Yan, B. Guan, J. Seely, B. Kjornrattanawanich, Highly sensitive visible-blind extreme ultraviolet Ni/4H-SiC Schottky photodiodes with large detection area, Optics letters 31 (2006) 1591–1593.

[7] N.G. Wright, A.B. Horsfall, SiC sensors: a review, J. Phys. D: Appl. Phys. 40 (2007) 6345–6354.

[8] M. Schraml, N. Papathanasiou, A. May, T. Weiss, T. Erlbacher, Towards Sic-Based VUV Pin-Photodiodes - Investigations on 4H-SiC Photodiodes with Shallow Implanted Al Emitters, KEM 947 (2023) 77–82.

[9] Synopsys Inc., Sentaurus™ Process: Version U-2022.12, 2022.

[10] Synopsys Inc., Sentaurus™ Device: Version U-2022.12, 2022.

[11] A. Burenkov, C.D. Matthus, T. Erlbacher, Optimization of 4H-SiC UV Photodiode Performance Using Numerical Process and Device Simulation, IEEE Sensors J. 16 (2016) 4246–4252.

[12] Synopsys Inc., Sentaurus™ Structure Editor: Version U-2022.12, 2022.

[13] O.P.A. Lindquist, K. Järrendahl, S. Peters, J.T. Zettler, C. Cobet, N. Esser, D.E. Aspnes, A. Henry, N.V. Edwards, Ordinary and extraordinary dielectric functions of 4H– and 6H–SiC from 3.5 to 9.0 eV, Appl. Phys. Lett. 78 (2001) 2715–2717.

[14] J. Weiße, M. Hauck, T. Sledziewski, M. Tschiesche, M. Krieger, A.J. Bauer, H. Mitlehner, L. Frey, T. Erlbacher, Analysis of Compensation Effects in Aluminum-Implanted 4H-SiC Devices, MSF 924 (2018) 184–187.

[15] Y.-x. Yuan, Recent advances in trust region algorithms, Math. Program. 151 (2015) 249–281.

[16] Synopsys Inc., Sentaurus™ Workbench Optimization Framework: Version U-2022.12, 2022